ChemComm

Influence of Donor Point Modifications on the Assembly of Chalcogen-Bonded Organic Frameworks

Journal:	*ChemComm*
Manuscript ID	CC-COM-10-2023-005162.R1
Article Type:	Communication

COMMUNICATION

Influence of Donor Point Modifications on the Assembly of Chalcogen-Bonded Organic Frameworks

Received 00th January 20xx,
Accepted 00th January 20xx

DOI: 10.1039/x0xx00000x

Brian J. Eckstein,[a] Hannah R. Martin,[a] Michael P. Moghadasnia,[a] Arijit Halder,[a] Michael J. Melville,[a] Tara N. Buzinski,[a] Gary J. Balaich[b] and C. Michael McGuirk*[a]

Incremental, single-atom substitutions of Se-based chalcogen bond (Ch-bond) donors with stronger donating Te centers were implemented in two new triptycene tris(1,2,5-chalcogenadiazole) tectons. The appreciably more favorable Ch-bonding ability of the Te-based donors promotes assembly of low-density networks and more stable Ch-bonded organic frameworks (ChOFs).

Synthetic porous frameworks encompass a structurally and functionally diverse collection of low-density materials typically classified by some characteristic mode of chemical bonding used to connect constituent building blocks into a 2D or 3D lattice. Owing to the intuitive structural and chemical modularity afforded by metal–ligand coordination and covalent bonding, metal–organic (MOFs) and covalent organic frameworks (COFs) are the most well-studied and well-developed classes of synthetic porous frameworks.[1, 2] Although constructing low-density structures through noncovalent interactions is considered by many an unreliable enterprise, considerable advancements have indeed been made with hydrogen-bonded (H-bonded) organic frameworks (HOFs).[3, 4] Among the canonical noncovalent interactions, the preferred directionality and strength of H-bonding enable assembly of interaction motifs (synthons) between molecular building blocks (tectons).[5] Importantly, each mode of connectivity uniquely shapes the respective framework properties,[2] and consequently no single class of framework—not MOFs , COFs, nor HOFs—is ideal for every possible application. Therefore, the exploration and development of emergent modes of intermolecular connectivity is essential to advancing the utility of synthetic framework materials towards meeting current, emergent, and future technological challenges.

Chalcogen bonding (Ch-bonding), is a recently recognized class of noncovalent interaction,[6] involving the attractive interaction between electrophilic regions induced on polarizable chalcogen atoms (donors) and nucleophilic sites of Lewis bases (acceptors).[6] While fundamentally analogous to H-bonding, several unique features make Ch-bonding especially attractive for deliberate noncovalent assembly, among them: Ch-bonding exhibits even greater preferred directionality than H-bonding; Ch-bond donors can be divalent, exhibiting two discrete electrophilic sites on a donor atom; and Ch-bonding strength can be modulated through donor atom substitution, varying with the chalcogen polarizability (Te > Se > S).[7] Moreover, the Ch-bonding properties of numerous synthetically accessible chalcogen-containing heterocycles have been studied, providing a basis for the development of Ch-bonding tectons for the assembly of low-density networks and porous frameworks.[8] Previous investigations into potential Ch-bonding tectons have examined triptycene tris(1,2,5-thiadiazole) and subsequently triptycene tris(1,2,5-selenadiazole) (**Trip3Sez**; Scheme 1, left), including work by our own group on the latter.[9, 10] These triptycene tris(1,2,5-chalcogenadiazole) structures were inspired by known H-bonding tectons, where the Ch-bond

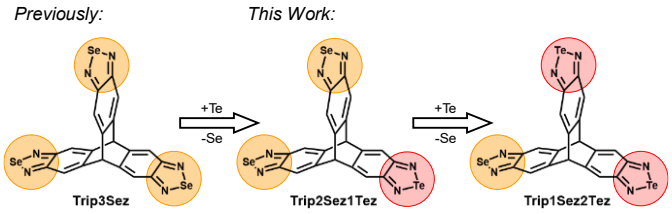

Scheme 1 Molecular structures of the triptycene tris(1,2,5-chalcogenadiazole) tectons **Trip3Sez** (left), reported previously, and **Trip2Sez1Tez** (centre) and **Trip1Sez2Tez** (right) studied in this work. The 1,2,5-selenadiazole (Sez) and 1,2,5-telluradiazole (Tez) moieties are highlighted by orange and red circles, respectively.

[a] *Department of Chemistry, Colorado School of Mines, Golden, Colorado, 80401, USA. E-mail: cmmcguirk@mines.edu*
[b] *Department of Chemistry & Chemistry Research Center, Laboratories for Advanced Materials, United States Airforce Academy, Colorado Springs, Colorado, 80840, USA.*

† Footnotes relating to the title and/or authors should appear here.
Electronic Supplementary Information (ESI) available: General and synthetic details, crystallographic methods and details for single-crystal and powder X-ray diffraction, figures and tables of structural information. CCDC 2301572, 2301573, and 2301581. See DOI: 10.1039/x0xx00000x

donor–acceptor pattern of 1,2,5-chalcogenadiazole moieties, in principle, enables extended assembly of anti-parallel $[Ch\cdots N]_2$ dimer synthons resembling polymeric H-bonding ribbon motifs found to template several low-density HOF structures.[3] Our studies with **Trip3Sez** revealed that the Ch-bonding assembly of the tecton is highly modular through solvent conditions, often affording diverse local and long-range structures.[10] For example, crystallization of **Trip3Sez** from dimethyl sulfoxide (DMSO) afforded a dense solvate structure that reveals solvent–tecton Ch-bonding interactions outcompete the desired dimeric $[Se\cdots N]_2$ connectivity between 1,2,5-selenadiazole (Sez) moieties (Fig. 1a,b). On the other hand, chloroaromatic solvents known to selectively disrupt π-stacking, such as 1-chloronaphthalene (CN), afforded **Trip3Sez**-*I*, a low-density Ch-bonded organic framework (ChOF) with hexagonal one-dimensional (1D) channels (Fig. 1c). We hypothesize the selective occupation of **Trip3Sez** π-faces by solvent promotes extended assembly of coplanar and symmetric $[Se\cdots N]_2$ dimers (Fig. 1c,d), with Se···N Ch-bonding distances ($d_{Se\cdots N}$) of ~2.9 Å, arranging the Sez moieties into polymeric ribbon motifs that template the desired honeycomb network topology. The **Trip3Sez**-*I* ChOF further demonstrated permeability to exchange between different chloroaromatic crystallization solvents, allowing it to be categorized as porous, but readily collapsed upon attempts to remove or exchange the chloroaromatic guests with more volatile solvents, such as acetone and pentane. The **Trip3Sez**-*I* ChOF represents an important precedent for Ch-bonding framework connectivity, yet the limited stability indicates considerably more work is necessary to advance Ch-bonding as a viable mode of porous, and permanently porous, framework connectivity.

To build directly upon our work with **Trip3Sez**, we sought to further study ChOF tectons with the same triptycene tris(1,2,5-chalcogenadiazole) molecular architecture, but stronger chalcogen bonding interactions. Sequential single atom substitutions, replacing Se with Te, was thus conceived as an approach to systematically examine the influences of increased Ch-bond donor strength on the assembly and stability of ChOF structures. Specifically, the interaction energies of 1,2,5-telluradiazole (Tez) $[Te\cdots N]_2$ dimers are expected to be over double that of Sez congeners[11] and comparable to urea and carboxylic acid dimeric H-bonding synthons.[12] Accordingly, we report herein the study of the assembly and stability of ChOFs with the mixed-donor Ch-bonding tectons triptycene bis(1,2,5-selenadiazole) mono(1,2,5-telluradiazole) (**Trip2Sez1Tez**; Scheme 1, centre) and triptycene mono(1,2,5-selenadiazole) bis(1,2,5-telluradiazole) (**Trip1Sez2Tez**; Scheme 1, right).

We first synthesized the **Trip2Sez1Tez** tecton, using a stepwise approach we developed to install Sez and then Tez moieties on a triptycene core (Schemes S1 and S2, ESI). Initial work with **Trip2Sez1Tez** notably revealed considerably diminished solubilities in conditions previously used with **Trip3Sez**. For example, **Trip2Sez1Tez** is effectively insoluble in chloroaromatic solvents and has roughly an order of magnitude lower solubility in DMSO relative to **Trip3Sez**. Consequently, early attempts to prepare sample solutions for NMR spectroscopy by heating **Trip2Sez1Tez** in DMSO-d_6 unexpectedly led to the crystallization of orange plates upon cooling. Characterization by single-crystal X-ray diffraction (SCXRD) revealed that **Trip2Sez1Tez** crystallizes from DMSO in the monoclinic space group *C*2/*c* to afford **Trip2Sez1Tez**-*VI*, featuring a new topology, distinct from the five reported in our previous work with **Trip3Sez** (i.e. *I*–*V*).[10] The structure comprises stacked ladder-like arrays of 1D channels, defined entirely through Ch-bonding connectivity, that host DMSO molecules too disordered to refine (Fig. 2a, center). The ladder "rungs" are formed by assembly of coplanar and symmetric $[Te\cdots N]_2$ dimers ($d_{Te\cdots N}$ = 2.73 Å; Fig. 2a, left), and the corrugated "rails" are formed by assembly of distorted $[Se\cdots N]_2$ dimers ($d_{Se\cdots N}$ = 2.89 and 2.91 Å; Fig. 2a, right).

The low-density and highly Ch-bonded structure of **Trip2Sez1Tez**-*VI* contrasts dramatically with **Trip3Sez**–DMSO (Fig. 1a, b), despite also crystallizing from DMSO, revealing the influence of the Te Ch-bond donor substitution on the hierarchical self-assembly of **Trip2Sez1Tez**. The significantly stronger Te···N Ch-bonding elevates the kinetics and stability of $[Te\cdots N]_2$ dimerization significantly above other competing solvent–tecton or tecton–tecton interactions, leading to rapid assembly of the Tez moieties into the coplanar ribbon motifs that hold the ladder-like arrays open. The resulting arrangement of **Trip2Sez1Tez** tectons promotes the extended dimeric $[Se\cdots N]_2$ assembly, which the **Trip3Sez**–DMSO structure indicates is otherwise unfavorable in DMSO. Intriguingly, the Sez ribbon motifs in **Trip2Sez1Tez**-*VI* are ultimately bent in accommodation of stacking interactions, apparently due to the weaker strength of Se···N Ch-bonding, relative to Te···N.

We then sought to identify crystallization conditions for **Trip2Sez1Tez** able to inhibit tecton–tecton stacking and thus promote assembly of an even lower-density structure. Recalling our previous work, CN was tested as a co-solvent in mixtures with DMSO. Additionally, *N*-methyl-2-pyrrolidinone (NMP) was

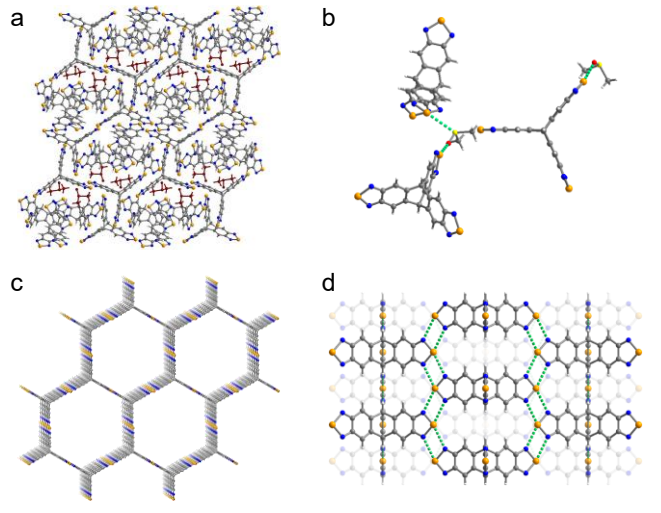

Fig. 1 Portions of the **Trip3Sez**–DMSO solvate crystal structure showing (a) the structure viewed along the [100] unit cell direction with DMSO molecules coloured dark red and (b) fragments highlighting the solvent–tecton Ch-bonding. Portions of the 1-chloronapthalene-solvated **Trip3Sez**-*I* ChOF crystal structure showing (c) the low-density hexagonal framework viewed just off the [001] unit cell direction and (d) the ribbon-like $[Se\cdots N]_2$ Ch-bonding connectivity viewed along the [210] unit cell direction. Unless otherwise noted, gold, yellow, red, blue, grey, and white spheres represent Se, S, O, N, C, and H atoms, respectively, and green dashed lines indicate Ch-bonding contacts.

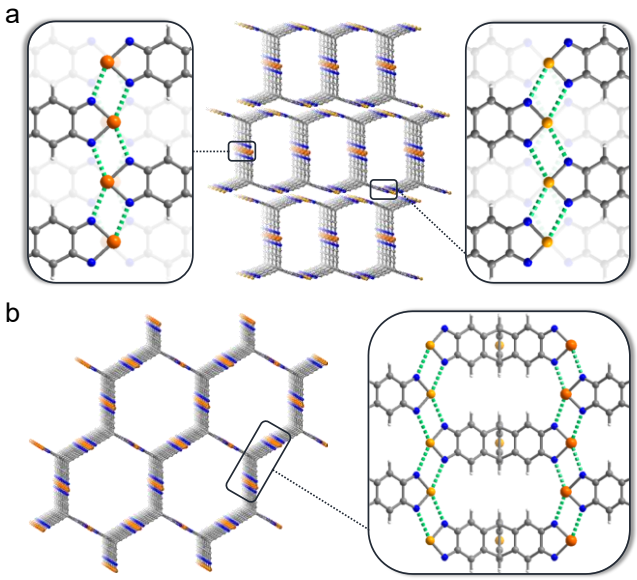

Fig. 2 (a) Portions of the **Trip2Sez1Tez**-*VI* crystal structure showing the staggered ladder-like arrays of 1D channels viewed along the [001] direction (centre) with callouts showing the Ch-bonding connectivity of the ideal $[Te\cdots N]_2$ dimers (left) and distorted $[Se\cdots N]_2$ dimers (right). (b) Portions of the **Trip2Sez1Tez**-*I* crystal structure showing the honeycomb structure viewed along the [001] direction with average 1/3 Te and 2/3 Se chalcogen atom occupancies (left) and a callout showing respective dimeric $[Te\cdots N]_2$ and $[Se\cdots N]_2$ Ch-bonding connectivity (right). Unless otherwise noted, orange, gold, blue, grey, and white spheres represent Te, Se, N, C, and H atoms, respectively, and green dashed lines indicate Ch-bonding contacts.

examined since it forms solvation shells with extensive stacking order,[13] which is correlated with an enhanced affinity for aromatic structures compared to related Lewis basic solvents.[14] Isostructural yellow needle-like single crystals were eventually obtained upon cooling hot solutions of **Trip2Sez1Tez** in either 1:4 CN–DMSO solvent mixtures or neat NMP. Characterization by SCXRD indicated that **Trip2Sez1Tez** crystallizes in the hexagonal space group $P6_3/mmc$ to afford **Trip2Sez1Tez**-*I*, which features the same honeycomb topology as **Trip3Sez**-*I* and hosts crystallization solvent molecules too disordered to refine (Fig. 2b, left). Note, **Trip2Sez1Tez**-*I* is an average structural solution wherein each 1,2,5-chalcogenadiazole has 2/3 Se and 1/3 Te occupancies. We expect the crystallization of **Trip2Sez1Tez**-*I* proceeds in hierarchical fashion where planar Tez ribbon motifs assemble first through rapid $[Te\cdots N]_2$ dimerization ($d_{Te\cdots N}$ = 2.73 Å; Fig. 2b, right), which is followed by the assembly of the Sez ribbon motifs through $[Se\cdots N]_2$ dimerization ($d_{Se\cdots N}$ = 2.81 Å; Fig. 2b, right). The Sez ribbon motifs can form with either cis- or trans- configurations with respect to the Tez ribbon motifs, which likely leads to disordered distributions of the chalcogen atoms (Fig. S11, ESI) that necessitate the spatially averaged structure solutions.

To characterize the porosity of **Trip2Sez1Tez**-*VI* and -*I*, batches of crystals of each structure were subject to series of solvent exchanges. Over the course of these experiments, powder X-ray diffraction (PXRD) and solution-phase ^{1}H NMR spectroscopy were used to monitor the batch-scale crystalline structure and pore guest content, respectively. Comparison of ^{1}H NMR spectra suggests the **Trip2Sez1Tez**-*VI* 1D channels are readily permeable to solvent exchanges from DMSO (crystallization solvent) to acetonitrile and then to diethyl ether (Fig. S12, ESI). However, significant variation between the corresponding PXRD patterns precludes any conclusion that the **Trip2Sez1Tez**-*VI* structure is maintained (Fig. S13, ESI). Plausibly, the weaker Ch-bonding strength of the distorted $[Se\cdots N]_2$ dimers and isotropic character of stacking interactions could enable facile structural rearrangements upon pore guest exchange.

Trip2Sez1Tez-*I* also exhibited guest permeability through complete exchanges from CN–DMSO (crystallization solvent) to acetone and then to *n*-pentane (Fig. S14, ESI). Gratifyingly, the corresponding PXRD patterns exhibit close agreement throughout (Fig. S15, ESI). The observed permeability can thus be correlated to the persistent hexagonal channel structure of **Trip2Sez1Tez**-*I*, establishing its porosity and classification as a ChOF.[10, 15] We then sought to demonstrate permanent porosity, but **Trip2Sez1Tez**-*I* exhibited significant loss of crystallinity upon removal of *n*-pentane and subsequently non-porous N_2 adsorption characteristics (Figs. S15 and S19a, ESI).

Encouraged by our findings with **Trip2Sez1Tez**, we proceeded to synthesize **Trip1Sez2Tez** by adapting the same stepwise approach used to obtain **Trip2Sez1Tez** (Schemes S1 and S3, ESI). The introduction of a second Te Ch-bond donor in **Trip1Sez2Tez** produces dramatic changes in solubility and crystallization kinetics. Specifically, **Trip1Sez2Tez** heated in DMSO, even at concentrations an order of magnitude lower than used for **Trip2Sez1Tez** NMR spectroscopy samples, leads to growth of fine, micron-scale yellow needle-like crystals upon cooling. Unfortunately, we have not found crystallization conditions for **Trip1Sez2Tez** in DMSO, or any other solvent, to grow sufficiently large crystals suitable for analysis by SCXRD. However, PXRD measurements along with the structural precedent set by analysis of single crystals of **Trip3Sez** and **Trip2Sez1Tez** do allow for structural characterization. Indeed, agreement with the PXRD patterns from as grown samples of **Trip3Sez**-*I* and **Trip2Sez1Tez**-*I* indicates that **Trip1Sez2Tez** crystallizes from DMSO in a structure, **Trip1Sez2Tez**-*I*, with the same honeycomb topology (Fig. 3), which corresponds to hexagonal 1D channels filled with solvent (Fig. 1c and Fig. 2b,

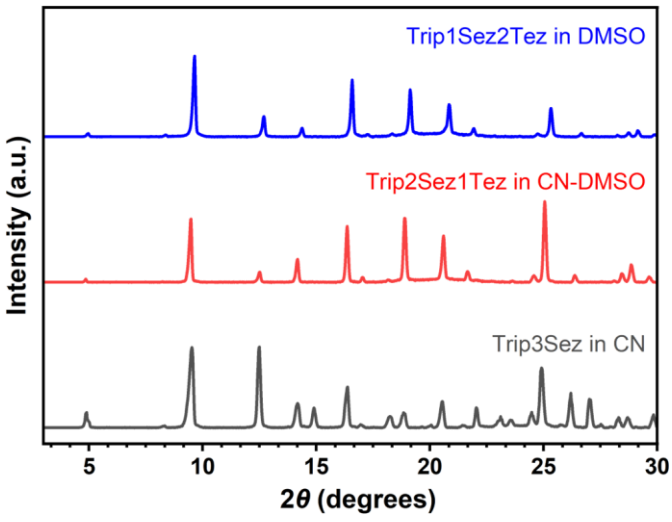

Fig. 3 Stacked powder X-ray diffraction (PXRD) patterns for "as grown" crystals of **Trip3Sez**-*I* in CN (dark grey), **Trip2Sez1Tez**-*I* in 1:4 CN–DMSO (red), and **Trip1Sez2Tez**-*I* in DMSO (blue).

left). Notably, this means that **Trip1Sez2Tez**-*I* can directly assemble into the honeycomb topology from strongly Lewis basic solvent and without conditions explicitly designed to inhibit π-stacking. The assembly of rigid and coplanar Tez ribbon motifs with two Te Ch-bond donors precludes large-area stacking interactions, and thus coplanar Sez ribbons form subsequently to maximize the Ch-bonding interaction energy of the $[Se\cdots N]_2$ dimers. Moreover, the strong $[Te\cdots N]_2$ dimerization strength precludes competition from DMSO.

Like **Trip2Sez1Tez**-*I*, ^{1}H NMR spectroscopy and PXRD confirm **Trip1Sez2Tez**-*I* exhibits porosity throughout solvent exchange experiments with acetone and then *n*-pentane (Figs. S16, S17a, and S18, ESI). Disappointingly, though, subsequent activation and gas adsorption experiments revealed that even with two Te Ch-bond donors, **Trip1Sez2Tez**-*I* failed to demonstrate permanent porosity upon solvent removal (Figs. S17b, S18 and S19b, ESI). Like **Trip2Sez1Tez**-*I*, the PXRD indicates the complete removal of guest solvent correlates with an apparent loss in crystallinity. We thus expect the loss in porosity likely corresponds to local amorphization that prevents pore access.

In conclusion, we have synthesized two new triptycene tris(1,2,5-chalcogenadiazole) tectons, **Trip2Sez1Tez** and **Trip1Sez2Tez**, featuring systematic single atom substitutions to examine the influences of Ch-bond donor strength on ChOF assembly and structure. Comparison of the DMSO-grown **Trip3Sez**–DMSO, **Trip2Sez1Tez**-*VI*, and **Trip1Sez2Tez**-*I* structures reveals how assembly of strong, coplanar $[Te\cdots N]_2$ dimers can template increasingly predictable, low-density structure. Two new ChOF structures, **Trip2Sez1Tez**-*I* and **Trip1Sez2Tez**-*I*, were confirmed through solvent exchange experiments. Though not permanently porous, stronger Te···N Ch-bonding enhances the stability of these ChOFs toward guest solvent exchange compared to isostructural **Trip3Sez**-*I*.

BJE and CMM conceptualized the work and supervised the investigations. BJE, HRM, MPM, AH, MJM, TMB, and GJB performed experiments and analysed the data. BJE wrote the original draft. All authors read and contributed to revisions.

This work was supported by the NSF DMR SSMC (Award #2143623) and start-up funds from Colorado School of Mines. This work made use of the IMSERC Crystallography facility at Northwestern University, which has received support from the Soft and Hybrid Nanotechnology Experimental (SHyNE) Resource (NSF ECCS-2025633), and Northwestern University. The authors thank Ed Dempsy for help collecting mass data and Dr. Charlotte Stern for collecting and solving SCXRD data.

Conflicts of interest

There are no conflicts to declare.

Notes and references

1 O. M. Yaghi, M. O'Keeffe, N. W. Ockwig, H. K. Chae, M. Eddaoudi and J. Kim, *Nature*, 2003, **423**, 705-714; M. J. Kalmutzki, N. Hanikel and O. M. Yaghi, *Sci. Adv.*, 2018, **4**, eaat9180; C. S. Diercks and O. M. Yaghi, *Science*, 2017, **355**, eaal1585; S. Li, X. Tan, M. Yue, L. Zhang, D. Chai, W. Wang, H. Pan, L. Fan and C. Zhao, *Chem. Commun.*, 2020, **56**, 15177-15180; S. Huang, B. Zhang, H. Sun, H. Hu, J. Wang, F. Duan, H. Zhu, M. Du and S. Lu, *Chem. Commun.*, 2023, **59**, 10424-10427.

2 A. G. Slater and A. I. Cooper, *Science*, 2015, **348**, aaa8075.

3 A. Pulido, L. Chen, T. Kaczorowski, D. Holden, M. A. Little, S. Y. Chong, B. J. Slater, D. P. McMahon, B. Bonillo, C. J. Stackhouse, A. Stephenson, C. M. Kane, R. Clowes, T. Hasell, A. I. Cooper and G. M. Day, *Nature*, 2017, **543**, 657-664; M. Mastalerz and I. M. Oppel, *Angew. Chem. Int. Ed.*, 2012, **51**, 5252-5255; B. Han, H. Wang, C. Wang, H. Wu, W. Zhou, B. Chen and J. Jiang, *J. Am. Chem. Soc.*, 2019, **141**, 8737-8740.

4 T.-H. Chen, I. Popov, W. Kaveevivitchai, Y.-C. Chuang, Y.-S. Chen, O. Daugulis, A. J. Jacobson and O. Š. Miljanić, *Nat. Commun.*, 2014, **5**, 5131; Q. Zhu, J. Johal, D. E. Widdowson, Z. Pang, B. Li, C. M. Kane, V. Kurlin, G. M. Day, M. A. Little and A. I. Cooper, *J. Am. Chem. Soc.*, 2022, **144**, 9893-9901; W. Yan, X. Yu, T. Yan, D. Wu, E. Ning, Y. Qi, Y.-F. Han and Q. Li, *Chem. Commun.*, 2017, **53**, 3677-3680.

5 I. Hisaki, C. Xin, K. Takahashi and T. Nakamura, *Angew. Chem. Int. Ed.*, 2019, **58**, 11160-11170; J. Luo, J.-W. Wang, J.-H. Zhang, S. Lai and D.-C. Zhong, *CrystEngComm*, 2018, **20**, 5884-5898.

6 C. B. Aakeroy, D. L. Bryce, G. R. Desiraju, A. Frontera, A. C. Legon, F. Nicotra, K. Rissanen, S. Scheiner, G. Terraneo, P. Metrangolo and G. Resnati, *Pure Appl. Chem.*, 2019, **91**, 1889-1892.

7 L. Vogel, P. Wonner and S. M. Huber, *Angew. Chem. Int. Ed.*, 2019, **58**, 1880-1891; P. Scilabra, G. Terraneo and G. Resnati, *Acc. Chem. Res.*, 2019, **52**, 1313-1324; K. T. Mahmudov, M. N. Kopylovich, M. F. C. Guedes da Silva and A. J. L. Pombeiro, *Dalton Trans.*, 2017, **46**, 10121-10138.

8 O. A. Rakitin and A. V. Zibarev, *Asian J. Org. Chem.*, 2018, **7**, 2397-2416; P. C. Ho, P. Szydlowski, J. Sinclair, P. J. W. Elder, J. Kübel, C. Gendy, L. M. Lee, H. Jenkins, J. F. Britten, D. R. Morim and I. Vargas-Baca, *Nat. Commun.*, 2016, **7**, 11299; A. F. Cozzolino, P. J. W. Elder and I. Vargas-Baca, *Coordination Chemistry Reviews*, 2011, **255**, 1426-1438.

9 B. Kohl, L. C. Over, T. Lohr, M. Vasylyeva, F. Rominger and M. Mastalerz, *Org. Lett.*, 2014, **16**, 5596-5599; S. Langis-Barsetti, T. Maris and J. D. Wuest, *J. Org. Chem.*, 2017, **82**, 5034-5045; W. Yang, R. Jiang, C. Liu, B. Yu, X. Cai and H. Wang, *Cryst. Growth Des.*, 2021, **21**, 6497-6503.

10 B. J. Eckstein, L. C. Brown, B. C. Noll, M. P. Moghadasnia, G. J. Balaich and C. M. McGuirk, *J. Am. Chem. Soc.*, 2021, **143**, 20207-20215.

11 A. F. Cozzolino and I. Vargas-Baca, *J. Organomet. Chem.*, 2007, **692**, 2654-2657; S. Scheiner, *J. Phys. Chem. A*, 2022, **126**, 1194-1203.

12 C. Colominas, J. Teixidó, J. Cemelí, F. J. Luque and M. Orozco, *J. Phys. Chem. B*, 1998, **102**, 2269-2276; D. Di Tommaso and K. L. Watson, *J. Phys. Chem. A*, 2014, **118**, 11098-11113; A. Bende, *Theor. Chem. Acc.*, 2009, **125**, 253-268.

13 N. S. Basma, T. F. Headen, M. S. P. Shaffer, N. T. Skipper and C. A. Howard, *J. Phys. Chem. B*, 2018, **122**, 8963-8971; A. Tagawa and T. Shikata, *Phys. Chem. Chem. Phys.*, 2019, **21**, 22081-22091.

14 W.-L. Xu, F. Mao, H.-K. Zhao, Y.-Q. Wang and J. Wang, *J. Chem. Eng. Data*, 2007, **52**, 553-554; N. F. Grishchenko, V. A. Rogozkin, I. I. Lastochkina and K. V. Golubeva, *Chem. Technol. Fuels Oils*, 1974, **10**, 762-764; Y. Hernandez, V. Nicolosi, M. Lotya, F. M. Blighe, Z. Sun, S. De, I. T. McGovern, B. Holland, M. Byrne, Y. K. Gun'Ko, J. J. Boland, P. Niraj, G. Duesberg, S. Krishnamurthy, R. Goodhue, J. Hutchison, V. Scardaci, A. C. Ferrari and J. N. Coleman, *Nat. Nanotechnol.*, 2008, **3**, 563-568.

15 L. J. Barbour, *Chem. Commun.*, 2006, 1163-1168.